EUROPEAN ORGANIZATION FOR NUCLEAR RESEARCH (CERN)

CERN-EP-2021-071
2022/04/29

CMS-HIN-18-011

Azimuthal correlations within exclusive dijets with large momentum transfer in photon-lead collisions

The CMS Collaboration

Abstract

The first measurement of the azimuthal angular correlations of exclusively produced events with two jets in photon-lead interactions at large momentum transfer is presented. Theoretical predictions relate such correlations to the polarization of gluons within nuclei. This study uses a data sample of lead-lead collisions at $\sqrt{s_{\mathrm{NN}}} = 5.02\,\mathrm{TeV}$, corresponding to an integrated luminosity of $0.38\,\mathrm{nb}^{-1}$, collected with the CMS experiment. One of the jets is required to have a transverse momentum above 30 GeV, while that of the second is greater than 20 GeV. The measured second harmonic of the correlation between the sum and difference of the two jet momenta is found to be positive, and rising, as the dijet momentum increases. The model representing the state-of-the-art calculations in electromagnetic interactions with protons overestimates this angular correlation. The measurement is also compared to a recent theoretical calculation that includes final state interactions.

Submitted to Physical Review Letters

Considerable experimental and theoretical effort is being devoted to the study of the momentum distribution of gluons in nuclei [1, 2]. The aim of such studies is to determine whether the distribution of low momentum gluons saturates, constituting a new state of matter. Accumulating evidence since early studies at BNL RHIC [3–6] points to a reduction of the density of low momentum gluons in heavy nuclei, as compared to the density in individual protons, at high energies. While experimental work has so far focused on one dimensional studies, the gluon distribution is intrinsically multidimensional, depending on impact parameter, transverse momentum and polarization [7].

Recent theoretical studies relate the multidimensional nature of gluons within nuclei to azimuthal angular correlations of final state jets produced in photon-hadron interactions [8–19]. The angular distribution dependance on gluon polarization remains almost completely unexplored. While the gluon polarization density matrices can be classified according to the Wigner or Husimi formalism [8–16], theoretical estimates of the magnitude of gluon polarization effects vary widely. These effects can be probed by measuring the second Fourier harmonic of the distribution of the azimuthal angle Φ between the sum and the difference of two jet momenta comprising a dijet [9]. Theory calculations relate this moment to the distribution of elliptically polarized gluons [12]. In this approach, the moment is a manifestation of non-trivial angular correlations of polarized gluons that depend on impact parameter and transverse momentum.

After a preliminary version of the current results was shown, a calculation based on final state radiation was found to result in a non-zero value for this harmonic, giving an alternative explanation for any observed correlations [20]. Experimental measurements are essential to resolve these two effects and to gain insight into the magnitude of gluon polarization within nuclei.

Photon-nucleus interactions can be produced using ultra-relativistic heavy-ion beams. At the CERN Large Hadron Collider, high energy lead (Pb) beams produce a large flux of virtual photons that can interact with an oncoming lead nucleus [21–23], in so-called ultra-peripheral heavy-ion collisions (UPC). The CMS collaboration has recently studied UPC exclusive vector meson photoproduction and photon-photon scattering [24–27]. The ALICE, ATLAS and LHCb collaborations have also recently reported on UPC measurements [28–30]. The CDF and ZEUS collaborations have studied exclusive dijet production in proton-antiproton [31] and diffractive electron-proton collisions [32], respectively. No published results exist on dijet production in photon-nucleus interactions.

This Letter reports the first measurement of $\langle\cos(2\Phi)\rangle$, where the brackets indicate an average over exclusive dijet events produced in photon–lead collisions. These events probe the large momentum transfer regime. In such events, the dijet and the incoming photon are typically moving in the same direction, and produced when the incoming photon fluctuates into a small color dipole, in comparison to the size of the nucleus. This dipole can then probe the interior of the Pb nucleus. Tabulated results are provided in the HEPData record for this analysis [33].

The central feature of the CMS apparatus is a superconducting solenoid of 6 m internal diameter, providing a magnetic field of 3.8 T. Within the solenoid volume are a silicon pixel and strip tracker, a lead tungstate crystal electromagnetic calorimeter (ECAL), and a brass and scintillator hadron calorimeter (HCAL). ECAL provides coverage in pseudorapidity $|\eta| < 1.48$ in a barrel (EB) region and $1.48 < |\eta| < 3.0$ in two endcap (EE) regions, while HCAL covers $|\eta| < 1.3$ for the barrel (HB) and $1.3 < |\eta| < 3.0$ for the two endcap (HE) sections, respectively. Detector elements in ECAL and HCAL are grouped into "towers." Hadron forward (HF) calorimeters extend the η coverage provided by the barrel and endcap detectors to $3.0 < |\eta| < 5.2$. The data sample is collected with a two-level trigger system [34]: at the hardware level events are selected by custom hardware processors, while a subsequent software trigger uses fast versions

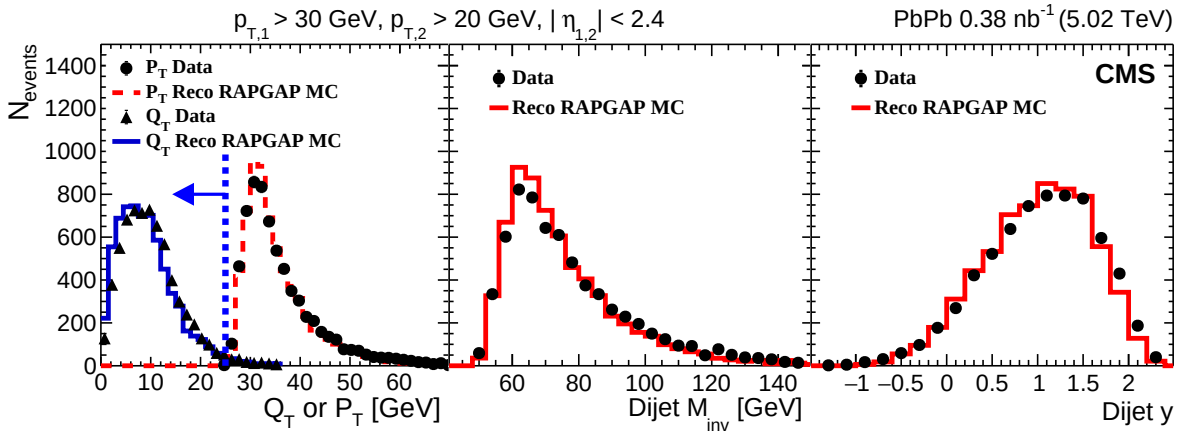

Figure 1: Magnitudes of the vector sum (Q_T) and vector difference (P_T) of the two jets (left). The dashed blue line illustrates the $Q_T < 25$ GeV requirement. Invariant mass (center) and rapidity (right) of the dijet candidates after all selection requirements. The lines show the RAPGAP MC generated events including detector resolution effects. The statistical uncertainties are covered by the symbol size.

of the offline reconstruction code. A detailed description of the CMS detector, together with a definition of the coordinate system used and the relevant kinematic variables, can be found in Ref. [35].

The analysis uses a data sample of lead-lead collisions at $\sqrt{s_{NN}} = 5.02$ TeV corresponding to an integrated luminosity of $0.38\,\text{nb}^{-1}$ collected in fall 2015. The average number of inelastic PbPb collisions per bunch crossing is about 0.01. Events are selected with a dedicated trigger designed to record a wide variety of photon-lead processes. The hardware trigger requires a transverse energy of at least 5 GeV in any of the ECAL towers, and at least one of the two HF calorimeters is required to not have a signal above the noise threshold. The software-based trigger requires at least one reconstructed track in the pixel detector. Since the charged particle multiplicities are low, events are reconstructed in the same way as if they were pp collisions. The primary vertex is required to be within 20 cm of the nominal center of the detector along the beam direction.

By combining information from all subdetectors, a particle-flow (PF) algorithm [36] attempts to identify all stable particles in an event, classifying them as electrons, muons, photons, and charged or neutral hadrons. Jets are reconstructed from these PF candidates using the anti-k_T algorithm [37] with a distance parameter of 0.4, as implemented in the FASTJET package [38]. The jet energy is calibrated by applying a multiplicative factor to relate, on average, the energy of the detector jet to that of the corresponding generator level particle jet (energy scale correction). The leading (subleading) jet is required to have a $p_T > 30\,(20)$ GeV.

The symmetry of the PbPb system leads to dijet events where the jets can travel in either direction through CMS. For the events of interest, the dijet is expected to be predominantly in the photon direction. This is taken as the "forward" direction. Events that have any additional jets with $p_T > 20$ GeV in either the forward or backward direction are rejected. Aside from the dijet tracks, both rapidity hemispheres are required to be devoid of hadronic activity. Events are discarded if they have an energy deposit in any of the calorimeter towers in the forward and backward rapidity hemispheres above the noise threshold (3.9/3.0/3.2 GeV in HF/HE/EE) [27].

A pseudorapidity gap is defined with $\Delta\eta^F = 2.4 - \eta_{\max}$, where 2.4 is the upper limit of the tracker and $\eta_{\max}$ is the maximum pseudorapidity of any high-purity charged track as defined in Ref. [39] and having $p_T > 0.2\,\text{GeV}$. A similar backward pseudorapidity gap $\Delta\eta^B$ is defined for the opposite η hemisphere. It is required that $\Delta\eta^B > \Delta\eta^F$ and that $\Delta\eta^B$ is greater than 1.2, effectively selecting dijet events that are located in the forward direction with a large rapidity gap as measured using the tracker. In addition, events with a PF candidate of more than 6 GeV in the forward hemisphere are rejected. Finally, one of the jets must be within one unit of pseudorapidity of the track defining the backward rapidity gap. Event samples with the dijet detected in either hemisphere of CMS are statistically independent and consistent with each other within 1% for the $\langle\cos(2\Phi)\rangle$. The samples are combined using the convention for defining the forward direction as described above. This means that we invert the rapidity sign for the sample having a backward going dijet. A total of 6785 dijet events remain after applying the above requirements.

In this analysis, the RAPGAP (version 3.303) [40] Monte Carlo (MC) generator, which was developed to explore electron-proton (ep) collisions, is used for comparisons with the experimental results and for studying sources of systematic uncertainties. The simulated events are processed and reconstructed in the same way as the collision data. GEANT4 [41] is used to account for the detector response. The simulated photon energy spectrum is rescaled to follow the photon distribution from lead nuclei of Ref. [42]. To avoid model-dependent assumptions, no additional modifications of the simulation have been made to account for differences between lead and proton dynamics. For the simulated events, 94% have the interacting photon and the dijet in the same hemisphere and, of these, 99% pass the selection criteria described above.

Based on the transverse momenta of the two jets relative to the beam axis, $\vec{p}_{T,1}$ and $\vec{p}_{T,2}$, the vector sum $\vec{Q}_T$ and vector difference $\vec{P}_T$ are defined, with $\vec{Q}_T = \vec{p}_{T,1} + \vec{p}_{T,2}$ and $\vec{P}_T = (\vec{p}_{T,1} - \vec{p}_{T,2})/2$ [8]. Theoretical calculations have focused on the "back-to-back" regime, i.e. $P_T > Q_T$ [43]. This requirement results in the rejection of 47 events (0.7% of the sample). Figure 1 shows the distributions of dijet Q_T, P_T, invariant mass, and rapidity for both data and reconstructed MC events. The good agreement between data and MC for the invariant mass and rapidity distributions suggests that the rescaling of the photon flux from ep to PbPb is reasonable. The measured Q_T distribution has its maximum at 9 GeV, which is well within the large momentum transfer regime.

To calculate the second moment of the azimuthal angle anisotropy, $\langle\cos(2\Phi)\rangle$, the angle Φ is obtained from the relation $\vec{P}_T \cdot \vec{Q}_T = |\vec{P}_T||\vec{Q}_T|\cos(\Phi)$. For the angular correlation measurements, the $\vec{p}_{T,1}$ and $\vec{p}_{T,2}$ vectors used to calculate $\vec{Q}_T$ and $\vec{P}_T$ are assigned randomly to the leading and subleading jets on an event-by-event basis. The dijet angular correlations are distorted compared to the underlying distributions by the acceptance and finite resolution of the detector. To correct for these effects, an unfolding procedure is used to estimate the parton-level distributions. The TUnfold [44] software package with the Tikhonov regularization method is used, where the strength of the regularization parameter is determined with the L-curve scan method by minimizing the average global correlation coefficient. The response matrix is evaluated by using simulated dijet events that pass all of the analysis requirements. The unfolding of the $dN/d\Phi$ distribution is performed for five equal intervals in $0 < Q_T < 25\,\text{GeV}$. The $\langle\cos(2\Phi)\rangle$ value is then calculated as a function of Q_T.

The following sources of systematic uncertainties on $\langle\cos(2\Phi)\rangle$ are considered: jet energy scale (JES) correction, JES nonclosure (JESnc), jet energy resolution (JER), jet η resolution (JPR), jet azimuthal angular resolution (JAR), trigger efficiency (TR), and the purity estimation (PUR). The uncertainty in the JES is 2% for jets with p_T of 20 GeV, as reported in Refs. [45, 46]. After the

nominal correction factors are applied, a small non-closure remains between the generator-level JES and that of the reconstructed jets. The systematic uncertainty from this effect is estimated by applying first a residual correction to the JES in simulation and then the dedicated selection requirements. The deviation from the nominal result is taken as an estimate of the systematic uncertainty. The simulation provides a JER of 14% for 20 GeV jets, decreasing slightly as a function of jet p_{T}, consistent with Refs. [45, 46]. The JAR and JPR are found to be 0.025 ± 0.005 (stat) and 0.015 ± 0.005 (stat), respectively, and are almost independent of p_{T} and η in the phase space relevant to this measurement. The uncertainties related to JER and JAR are estimated from the differences between the resolution in data and MC as done in Ref. [45]. For this estimate, the detector-level jets in the simulation are broadened in order to account for the observed resolution in data. The $\langle\cos(2\Phi)\rangle$ uncertainty related to the JPR is found to be negligible.

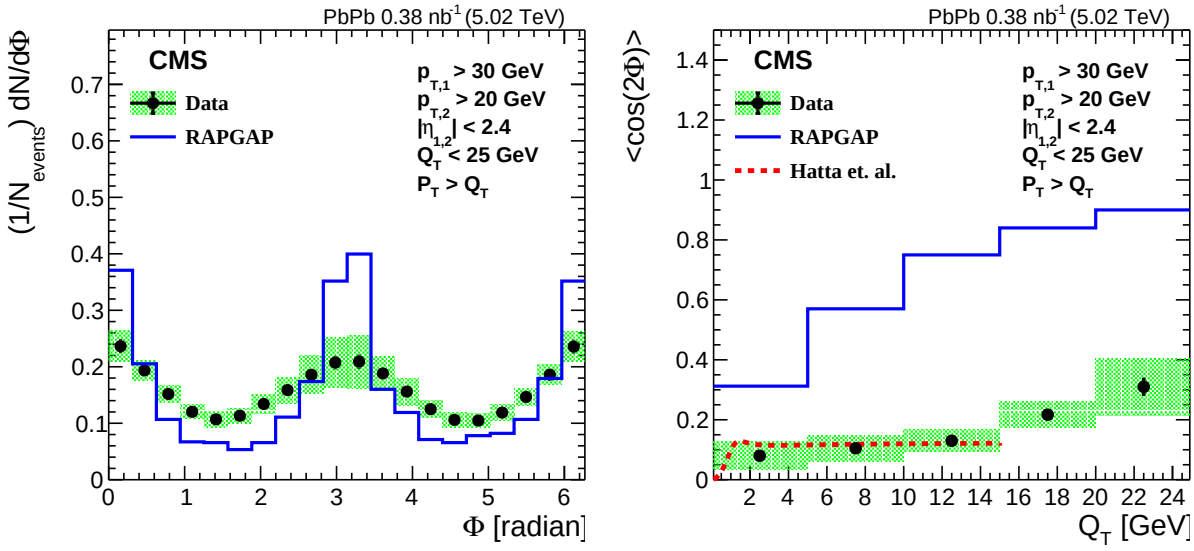

Figure 2: The unfolded $(1/N_{\mathrm{events}})\mathrm{d}N/\mathrm{d}\Phi$ distribution (left) and the unfolded $\langle\cos(2\Phi)\rangle$ values as a function of Q_{T} (right). The corresponding distributions from the RAPGAP simulation at the generator level (blue lines) and theoretical calculation by H. Hatta et al. [20] for $\langle\cos(2\Phi)\rangle$ (red dashed lines) are also shown. The dijet events are found predominantly in the "forward" direction, the $0 < \eta_{\mathrm{jet}} < 2.4$ range. Both the statistical (error bars) and systematic (green boxes) uncertainties are shown.

The uncertainty related to the purity of the signal (PUR) is estimated by varying the nominal pseudorapidity gap requirement between 0 and 2, and by varying the requirement for the minimal distance in pseudorapidity between the track defining the backward pseudorapidity gap and the nearest jet, which has a nominal value of 1.0, from 0.8 to 1.2. Increasing the threshold on the total energy of the PF candidates outside the jet cones from 6.0 to 6.6 GeV has a negligible effect on the purity uncertainty. The uncertainty associated with the trigger efficiency (TR) is related to the component that requires the transverse energy in one of the ECAL towers to be larger than 5 GeV. This requirement tends to slightly increase the fraction of electromagnetic energy in the jets. To account for this effect, simulated events are weighted by the trigger efficiency as a function of jet p_{T} on an event-by-event basis. This weighting reproduces the effect of the trigger efficiency on the measured $\langle\cos(2\Phi)\rangle$ values. The other elements forming the trigger, discussed above, are fully efficient. The uncertainties related to the calorimeter exclusivity selections and to the unfolding procedure are negligible. The various components of the $\langle\cos(2\Phi)\rangle$ distribution systematic uncertainties are summarized in Table 1.

Table 1: Table of $\langle\cos(2\Phi)\rangle$ systematic uncertainties (absolute values). The individual components are discussed in the text.

Q_T [GeV]	JES	JESnc	JER	JAR	PUR	TR	Total
0-5	0.018	0.004	0.002	0.004	0.002	0.004	0.019
5-10	0.012	0.006	0.005	0.003	0.002	0.003	0.015
10-15	0.010	0.008	0.007	0.002	0.002	0.001	0.014
15-20	0.009	0.008	0.014	0.002	0.002	0.001	0.018
20-25	0.005	0.018	0.056	0.001	0.002	0.002	0.059

Figure 2 (left) shows the unfolded angular distribution $dN/d\Phi$ for $Q_T < 25\,\text{GeV}$. The $dN/d\Phi$ distribution peaks at 0 and π, implying a positive value of $\langle\cos(2\Phi)\rangle$. This phenomenon is not a trivial acceptance effect as demonstrated by performing the analysis upon pairs of jets from different events, yielding the expected negative value of $\langle\cos(2\Phi)\rangle$ [13]. Figure 2 (right) shows that $\langle\cos(2\Phi)\rangle$ rises steadily with Q_T. The data have been compared to two different calculations that ignore the effect of elliptically polarized gluons. A calculation based on the RAPGAP model [40], which is tuned to HERA results and considers unpolarized gluon distributions, predicts that $\langle\cos(2\Phi)\rangle$ rises with Q_T, but overshoots the data by a factor of three. A calculation by Hatta et al. [20], which assumes soft gluon radiation from final state jets as the dominant effect of the azimuthal anisotropy, has $\langle\cos(2\Phi)\rangle$ initially rising, but then plateauing for $Q_T > 1\,\text{GeV}$.

In summary, the exclusive production of two jets in photon-lead interactions with a large rapidity gap has been studied for the first time. Events are characterized by a momentum transfer much larger than in previous measurements of exclusive production in photon-lead interactions. The second harmonic of the angular correlation between the sum and difference of the two jet momenta is found to be positive, and rising with dijet momentum in the measured range 0 to 25 GeV. The RAPGAP model, which has been successful at describing a wide range of HERA data, overestimates the strength of the correlations. An a posteriori calculation that includes the effect of soft-gluon radiation from final state interactions is able to describe the average magnitude of the correlations for dijet momentum less than 15 GeV. However, this calculation plateaus above 1 GeV, in contrast to the steady rise observed in the data. These results call for new calculations to elucidate the strength of gluon polarization in nuclear targets.

References

[1] J. L. Albacete and C. Marquet, "Gluon saturation and initial conditions for relativistic heavy ion collisions", *Prog. Part. Nucl. Phys.* **76** (2014) 1, doi:10.1016/j.ppnp.2014.01.004, arXiv:1401.4866.

[2] R. Abdul Khalek et al., "Science requirements and detector concepts for the Electron-Ion Collider: EIC yellow report", 2021. arXiv:2103.05419.

[3] BRAHMS Collaboration, "Evolution of the nuclear modification factors with rapidity and centrality in dAu collisions at $\sqrt{s_{NN}} = 200$ GeV", *Phys. Rev. Lett.* **93** (2004) 242303, doi:10.1103/PhysRevLett.93.242303, arXiv:nucl-ex/0403005.

[4] STAR Collaboration, "Forward neutral pion production in pp and dAu collisions at $\sqrt{s_{NN}} = 200$ GeV", *Phys. Rev. Lett.* **97** (2006) 152302, doi:10.1103/PhysRevLett.97.152302, arXiv:nucl-ex/0602011.

[5] PHENIX Collaboration, "Suppression of back-to-back hadron pairs at forward rapidity in dAu collisions at $\sqrt{s_{\rm NN}} = 200$ GeV", *Phys. Rev. Lett.* **107** (2011) 172301, doi:10.1103/PhysRevLett.107.172301, arXiv:1105.5112.

[6] PHOBOS Collaboration, "High transverse momentum triggered correlations over a large pseudorapidity acceptance in AuAu collisions at $\sqrt{s_{\rm NN}} = 200$ GeV", *Phys. Rev. Lett.* **104** (2010) 062301, doi:10.1103/PhysRevLett.104.062301, arXiv:0903.2811.

[7] M. Diehl, "Introduction to GPDs and TMDs", *Eur. Phys. J. A* **52** (2016) 149, doi:10.1140/epja/i2016-16149-3, arXiv:1512.01328.

[8] T. Altinoluk, N. Armesto, G. Beuf, and A. H. Rezaeian, "Diffractive dijet production in deep inelastic scattering and photon-hadron collisions in the color glass condensate", *Phys. Lett. B* **758** (2016) 373, doi:10.1016/j.physletb.2016.05.032, arXiv:1511.07452.

[9] Y. Hatta, B.-W. Xiao, and F. Yuan, "Probing the small-x gluon tomography in correlated hard diffractive dijet production in deep inelastic scattering", *Phys. Rev. Lett.* **116** (2016) 202301, doi:10.1103/PhysRevLett.116.202301, arXiv:1601.01585.

[10] Y. Hagiwara et al., "Accessing the gluon Wigner distribution in ultraperipheral pA collisions", *Phys. Rev. D* **96** (2017) 034009, doi:10.1103/PhysRevD.96.034009, arXiv:1706.01765.

[11] Y. Hatta, B.-W. Xiao, and F. Yuan, "Gluon tomography from deeply virtual Compton scattering at small-x", *Phys. Rev. D* **95** (2017) 114026, doi:10.1103/PhysRevD.95.114026, arXiv:1703.02085.

[12] H. Mantysaari, N. Mueller, and B. Schenke, "Diffractive dijet production and Wigner distributions from the color glass condensate", *Phys. Rev. D* **99** (2019) 074004, doi:10.1103/PhysRevD.99.074004, arXiv:1902.05087.

[13] A. Dumitru, V. Skokov, and T. Ullrich, "Measuring the Weizsacker-Williams distribution of linearly polarized gluons at an electron-ion collider through dijet azimuthal asymmetries", *Phys. Rev. C* **99** (2019) 015204, doi:10.1103/PhysRevC.99.015204, arXiv:1809.02615.

[14] Y. Hagiwara, Y. Hatta, and T. Ueda, "Wigner, Husimi, and generalized transverse momentum dependent distributions in the color glass condensate", *Phys. Rev. D* **94** (2016) 094036, doi:10.1103/PhysRevD.94.094036, arXiv:1609.05773.

[15] Y. Hagiwara, Y. Hatta, B.-W. Xiao, and F. Yuan, "Elliptic flow in small systems due to elliptic gluon distributions?", *Phys. Lett. B* **771** (2017) 374, doi:10.1016/j.physletb.2017.05.083, arXiv:1701.04254.

[16] J. Zhou, "Elliptic gluon generalized transverse-momentum-dependent distribution inside a large nucleus", *Phys. Rev. D* **94** (2016) 114017, doi:10.1103/PhysRevD.94.114017, arXiv:1611.02397.

[17] M. Strikman, R. Vogt, and S. N. White, "Probing small-x parton densities in ultraperipheral AA and pA collisions at the CERN Large Hadron Collider", *Phys. Rev. Lett.* **96** (2006) 082001, doi:10.1103/PhysRevLett.96.082001, arXiv:hep-ph/0508296.

[18] V. Guzey and M. Klasen, "Diffractive dijet photoproduction in ultraperipheral collisions at the LHC in next-to-leading order QCD", *JHEP* **04** (2016) 158, doi:10.1007/JHEP04(2016)158, arXiv:1603.06055.

[19] P. Kotko et al., "Estimating nonlinear effects in forward dijet production in ultra-peripheral heavy ion collisions at the LHC", *Eur. Phys. J. C* **77** (2017) 353, doi:10.1140/epjc/s10052-017-4906-6, arXiv:1702.03063.

[20] Y. Hatta, B.-W. Xiao, F. Yuan, and J. Zhou, "Anisotropy in dijet production in exclusive and inclusive processes", *Phys. Rev. Lett.* **126** (2021) 142001, doi:10.1103/PhysRevLett.126.142001, arXiv:2010.10774.

[21] A. J. Baltz et al., "The physics of ultraperipheral collisions at the LHC", *Phys. Rept.* **458** (2008) 1, doi:10.1016/j.physrep.2007.12.001, arXiv:0706.3356.

[22] J. G. Contreras and J. D. Tapia Takaki, "Ultra-peripheral heavy-ion collisions at the LHC", *Int. J. Mod. Phys. A* **30** (2015) 1542012, doi:10.1142/S0217751X15420129.

[23] S. Klein and P. Steinberg, "Photonuclear and two-photon interactions at high-energy nuclear colliders", *Ann. Rev. Nucl. Part. Sci.* **70** (2020) 323, doi:10.1146/annurev-nucl-030320-033923, arXiv:2005.01872.

[24] CMS Collaboration, "Coherent J/ψ(1S) photoproduction in ultra-peripheral PbPb collisions at $\sqrt{s_{\mathrm{NN}}} = 2.76$ TeV with the CMS experiment", *Phys. Lett. B* **772** (2017) 489, doi:10.1016/j.physletb.2017.07.001, arXiv:1605.06966.

[25] CMS Collaboration, "Measurement of exclusive $\rho(770)$ photoproduction in ultraperipheral pPb collisions at $\sqrt{s_{\mathrm{NN}}} = 5.02$ TeV", *Eur. Phys. J. C* **79** (2019) 702, doi:10.1140/epjc/s10052-019-7202-9, arXiv:1902.01339.

[26] CMS Collaboration, "Measurement of exclusive Υ photoproduction from protons in pPb collisions at $\sqrt{s_{\mathrm{NN}}} = 5.02$ TeV", *Eur. Phys. J. C* **79** (2019) 277, doi:10.1140/epjc/s10052-019-6774-8, arXiv:1809.11080.

[27] CMS Collaboration, "Evidence for light-by-light scattering and searches for axion-like particles in ultraperipheral PbPb collisions at $\sqrt{s_{\mathrm{NN}}} = 5.02$ TeV", *Phys. Lett. B* **797** (2019) 134826, doi:10.1016/j.physletb.2019.134826, arXiv:1810.04602.

[28] ALICE Collaboration, "Coherent J/ψ(1S) photoproduction in ultra-peripheral PbPb collisions at $\sqrt{s_{\mathrm{NN}}} = 2.76$ TeV", *Phys. Lett. B* **718** (2013) 1273, doi:10.1016/j.physletb.2012.11.059, arXiv:1209.3715.

[29] ATLAS Collaboration, "Observation of light-by-light scattering in ultraperipheral PbPb collisions with the ATLAS detector", *Phys. Rev. Lett.* **123** (2019) 052001, doi:10.1103/PhysRevLett.123.052001, arXiv:1904.03536.

[30] LHCb Collaboration, "Central exclusive production of J/ψ(1S) and ψ(2S) mesons in pp collisions at $\sqrt{s} = 13$ TeV", *JHEP* **10** (2018) 167, doi:10.1007/JHEP10(2018)167, arXiv:1806.04079.

[31] CDF Collaboration, "Observation of exclusive dijet production at the fermilab tevatron $\mathrm{p\overline{p}}$ collider", *Phys. Rev. D* **77** (2008) 052004, doi:10.1103/PhysRevD.77.052004, arXiv:0712.0604.

[32] ZEUS Collaboration, "Production of exclusive dijets in diffractive deep inelastic scattering at HERA", *Eur. Phys. J. C* **76** (2016) 16, doi:10.1140/epjc/s10052-015-3849-z, arXiv:1505.05783.

[33] HEPData record for this analysis, 2022. doi:10.17182/hepdata.95235.

[34] CMS Collaboration, "The CMS trigger system", *JINST* **12** (2017) P01020, doi:10.1088/1748-0221/12/01/P01020, arXiv:1609.02366.

[35] CMS Collaboration, "The CMS experiment at the CERN LHC", *JINST* **3** (2008) S08004, doi:10.1088/1748-0221/3/08/S08004.

[36] CMS Collaboration, "Particle-flow reconstruction and global event description with the CMS detector", *JINST* **12** (2017) P10003, doi:10.1088/1748-0221/12/10/P10003, arXiv:1706.04965.

[37] M. Cacciari, G. P. Salam, and G. Soyez, "The anti-k_{T} jet clustering algorithm", *JHEP* **04** (2008) 063, doi:10.1088/1126-6708/2008/04/063, arXiv:0802.1189.

[38] M. Cacciari, G. P. Salam, and G. Soyez, "FastJet user manual", *Eur. Phys. J. C* **72** (2012) 1896, doi:10.1140/epjc/s10052-012-1896-2, arXiv:1111.6097.

[39] CMS Collaboration, "CMS tracking performance results from early LHC operation", *Eur. Phys. J. C* **70** (2010) 1165, doi:10.1140/epjc/s10052-010-1491-3, arXiv:1007.1988.

[40] H. Jung, "Hard diffractive scattering in high-energy ep collisions and the Monte Carlo generator RAPGAP", *Comput. Phys. Commun.* **86** (1995) 147, doi:10.1016/0010-4655(94)00150-Z.

[41] GEANT4 Collaboration, "GEANT4: A simulation toolkit", *Nucl. Instrum. Meth. A* **506** (2003) 250, doi:10.1016/S0168-9002(03)01368-8.

[42] S. R. Klein et al., "STARlight: A Monte Carlo simulation program for ultra-peripheral collisions of relativistic ions", *Comput. Phys. Commun.* **212** (2017) 258, doi:10.1016/j.cpc.2016.10.016, arXiv:1607.03838.

[43] S. R. Klein and H. Mantysaari, "Imaging the nucleus with high-energy photons", *Nature Rev. Phys.* **1** (2019) 662, doi:10.1038/s42254-019-0107-6, arXiv:1910.10858.

[44] S. Schmitt, "TUnfold: an algorithm for correcting migration effects in high energy physics", *JINST* **7** (2012) T10003, doi:10.1088/1748-0221/7/10/T10003, arXiv:1205.6201.

[45] CMS Collaboration, "Jet energy scale and resolution in the CMS experiment in p p collisions at 8 TeV", *JINST* **12** (2017), no. 02, P02014, doi:10.1088/1748-0221/12/02/P02014, arXiv:1607.03663.

[46] CMS Collaboration, "Constraining gluon distributions in nuclei using dijets in proton-proton and proton-lead collisions at $\sqrt{s_{\mathrm{NN}}} = 5.02$ TeV", *Phys. Rev. Lett.* **121** (2018) 062002, doi:10.1103/PhysRevLett.121.062002, arXiv:1805.04736.